

THE 4TH INTERNATIONAL CONFERENCE ON ALUMINUM ALLOYS

STRESS CORROSION CRACK PROPAGATION IN ALUMINIUM ALLOY 7150

T.J. Warner¹, S.B. Newcomb² and W.M. Stobbs²

¹ Pechiney CRV, BP 27, 38340 Voreppe, France

² Department of Materials Science and Metallurgy, Cambridge University, Pembroke Street, Cambridge, CB2 3QZ, UK

Abstract

Stress corrosion crack propagation in peak aged and overaged 7150 alloy has been characterised by transmission electron microscopy (TEM) and optical microscopy cross-sections, as well as by fractographic examination of the failure surfaces in scanning electron microscopy. The crack tip is localised at or within a couple of nanometres of the grain boundary in the T651 temper, and at about 1 μm from grain boundaries in the T7451 crack tips examined. Crack propagation takes place in the L-LT plane, irrespective of loading direction between 0 and 45° to the ST direction. Although the alloy failed in conditions favouring hydrogen embrittlement, no particular evidence for gross hydrogen embrittlement was obtained from the microstructural characterisations.

1. Introduction

Stress corrosion cracking of Al-Zn-Mg-Cu alloys has been the subject of a considerable number of papers and reviews (e.g. [1]-[3]) in recent years. Although there is no consensus on the precise mechanism of SCC, most investigators attribute crack propagation to hydrogen embrittlement or stress assisted anodic dissolution. Among the difficulties encountered in identifying the operative mechanism(s) is the difficulty in following the crack propagation processes, which are inherently local and take place in the bulk of the material, except by indirect or macroscopic means.

In order to study the parameters controlling stress corrosion cracking, a number of researchers have correlated microstructural modifications of copper-rich 7xxx alloys during overaging with the corresponding improvements in their macroscopic SCC resistances. The grain boundary microstructures, in particular, have received considerable attention: the grain boundary precipitates' size, shape, and density, the precipitate free zones' size and composition, and other derived parameters, have all been correlated with macroscopic indicators of stress corrosion performance (e.g. [4]-[8]). Other authors have concentrated on the changes in the characteristics of intragranular precipitates during overaging (e.g. [9]) or changes in dislocation densities (e.g. [10]) to account for the improvements in SCC performance. Although these observations often provide good correlations between microstructural parameters and SCC resistance, the corresponding causal relationships have not been unambiguously identified.

Another approach to distinguishing between dominant SCC mechanisms involves the use of particular loading modes or sequences, or performing tests under impressed electrochemical potentials to favour particular propagation modes. Thompson et al [11], for example, have compared stress corrosion cracking in Mode I and Mode III loading of 7075 alloy, arguing that

hydrogen embrittlement is favoured by the triaxial stress state encountered in Mode I and considerably less favoured in Mode III. Other authors have encouraged hydrogen embrittlement processes by hydrogen charging (e.g. [12]) or by performing tests at cathodic potentials (e.g. [13]). Overall these studies demonstrate the sensitivity of copper-rich 7xxx alloys to SCC under conditions that favour hydrogen embrittlement, but do not rule out anodic dissolution mechanisms (or even postulate them [11]) for other loading modes or electrochemical potentials. The main purpose of the present study was to characterise the geometry and chemistry of crack propagation in 7150 alloy directly by microstructural analysis (optical microscopy, scanning electron microscopy (SEM), and transmission electron microscopy (TEM)) of stress corrosion cracked specimens. The aim was to interpret these observations in terms of the models that are proposed for SCC in the scientific literature.

2. Experimental Methods

The 7150 aluminium alloy tested in this study was supplied by Pechiney Rhenalu's Issoire plant in the form of 38 mm plate in the T351 temper. The T651 and T7451 ageing treatments were subsequently performed in the laboratory at Pechiney CRV.

Stress corrosion testing was performed in constant load experiments with alternate immersion in 3.5% NaCl according to ASTM standards G44 and G49. The specimens used were of 4 mm diameter and were cut at a number of angles to the ST direction: 0° (ST), 30°, 45°, and 90° (LT direction). Three specimens were tested at each of the stress levels studied.

In order to study the possible effect of hydrogen embrittlement on these tempers, ST specimens were tested as continuously immersed in aerated 3.5% NaCl at free potential or at an impressed cathodic potential of -1100 mV/SCE (favouring hydrogen embrittlement processes at the expense of anodic dissolution) at stresses at which they failed in alternate immersion tests (75 MPa for the T651 temper, 325 MPa for the T7451 temper). By analogy with Najjar et al's [13] slow strain rate experiments involving pre-corrosion of specimens to encourage hydrogen embrittlement at defects in the metal, specimens were tested with or without a short pre-exposure to a standard SCC test (0 or 1 day for the T651 temper, 0 or 4 days for the T7451 temper).

The TEM foils were prepared using standard ion beam milling techniques on "edge-on" specimens [14]. The foils were milled until a region containing a crack tip was thin enough to be characterised, and then examined in a Jeol 2000 FX.

3. Results

3.1 Stress corrosion crack propagation as a function of orientation

The times to failure in the constant load experiments for the four specimen orientations are shown in figure 1. Estimations of SCC threshold stresses that can be deduced from these data are plotted as a function of specimen orientation in figure 2. The most sensitive direction to SCC is, as expected, the ST direction. For both tempers the threshold stresses are slightly greater at 30° and 45° with respect to the ST direction and then increase to considerably higher levels in the LT direction. The correlations between the estimated thresholds at 0-45° and a fitted $\sigma(0^\circ)/\cos\theta$ curve are good for both T651 and T7451 tempers (on the assumption, thus, that the resolved stress in the direction perpendicular to the crack propagation plane, in this case the ST direction, controls crack propagation).

Corresponding cross-sectional optical micrographs at 45° to the ST direction in the ST-LT plane are presented in figures 3 and 4 for the T651 and T7451 tempers respectively. Irrespective of temper or specimen angle, it is clear that on an optical scale crack propagation takes place at grain boundaries in the L-LT plane. The presence of sub-grain boundaries that are mechanically

favourably oriented does not alter the crack propagation direction. The crack tips are considerably finer in the T651 specimens than in the T7451 specimens. Moreover, many cracks of lengths greater than 200 μm were observed along the lengths of the T651 specimens, consistent with the very low resistance of this temper to SCC.

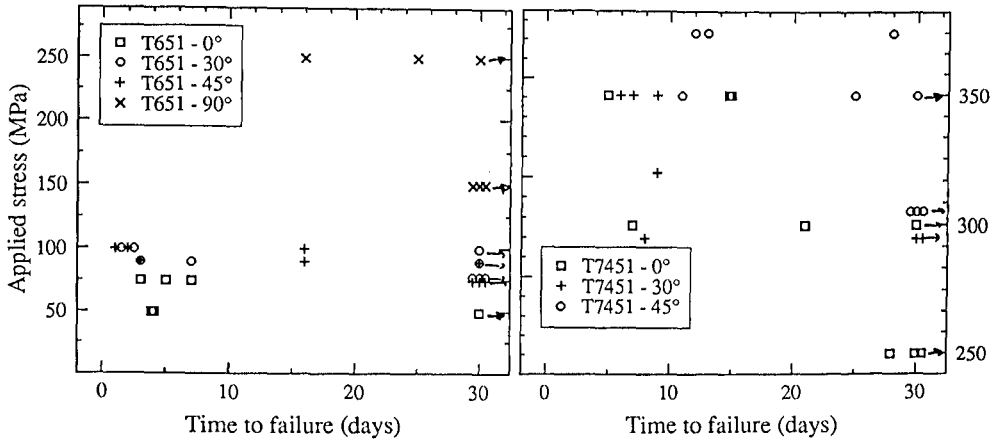


Figure 1. Applied stress versus time to failure for 7150-T651 and 7150-T7451 alloys for specimens cut at 0°, 30°, 45°, and 90° (LT) to the ST direction of 38 mm plate.

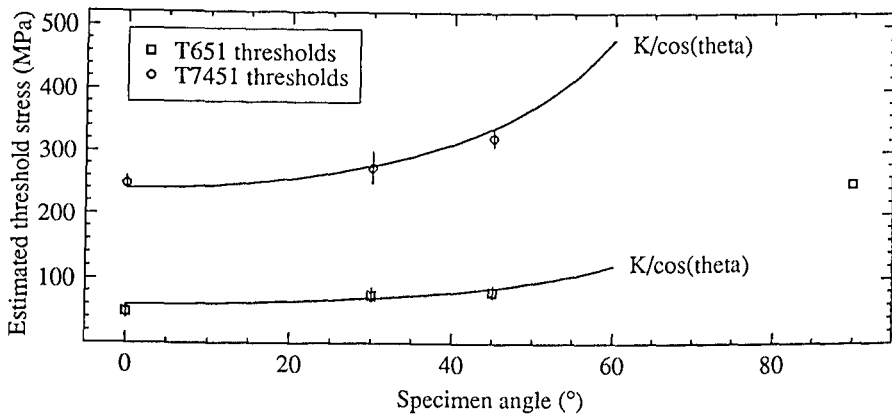


Figure 2. Estimated threshold stresses as a function of specimen orientation. The 0-45° thresholds appear consistent with a fitted $\sigma(0^\circ)/\cos\theta$ curve for both T651 and T7451 tempers, i.e. with the assumption that the resolved stress in the ST direction controls crack propagation.

SEM micrographs of regions characteristic of the environmentally-induced cracking at all angles except 90° are presented in figures 5a and 5b for the T651 and the T7451 tempers respectively. The fracture surfaces are indicative of failure at or near grain boundaries. On the T651 specimens, the fracture surface is decorated with subsidiary cracks that are consistent with inter-sub-granular corrosion after passage of the primary stress corrosion crack (see figure 5a). These

are less frequent for the T7 temper, the fracture surface of which shows surface faceting indicating generalised corrosion in an acid environment after passage of a stress corrosion crack.

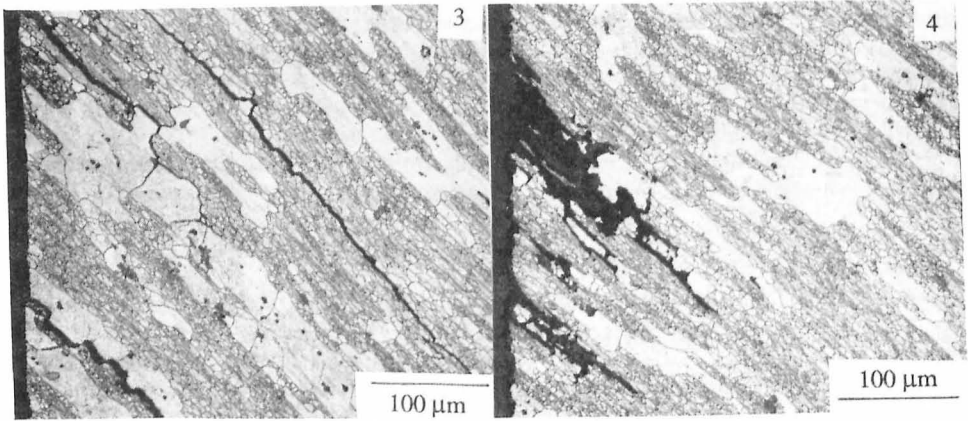


Figure 3. Cross-sectional optical micrograph in the LT-ST plane showing SCC in a T651 specimen cut at 45° to the ST direction. The crack propagation in the L-LT plane is characteristic of the 0-45° specimen orientations (chromic etch).

Figure 4. Cross-sectional optical micrograph in the LT-ST plane showing SCC in a T7451 specimen cut at 45° to the ST direction. The crack propagation in the L-LT plane is characteristic of the 0-45° specimen orientations (chromic etch).

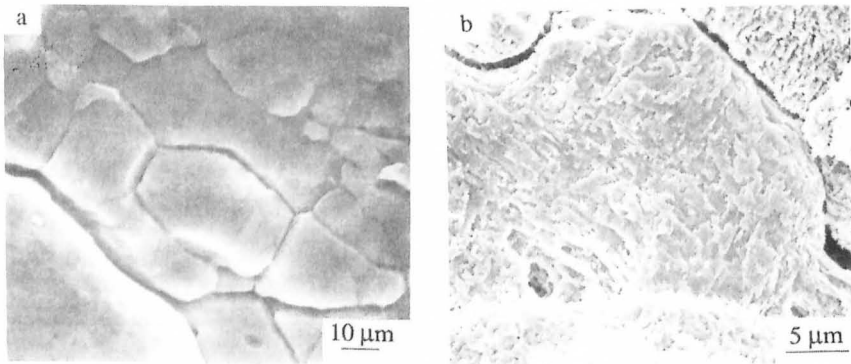


Figure 5. Characteristic SEM micrographs of fracture surfaces in the (a) T651 and (b) T7451 tempers of specimens cut in the ST direction. Note the brittle intergranular crack propagation with inter-subgranular corrosive attack for the T651 temper, and faceting characteristic of acid attack in the T7451 temper.

3.2 Stress corrosion cracking by hydrogen embrittlement

The results of the SCC corrosion tests under continuous immersion with or without an impressed cathodic potential are presented in table I. The only specimens that show failures are those that were tested at an impressed cathodic potential after pre-exposure, i.e. in conditions favouring hydrogen embrittlement. Examination of the fracture surfaces of these specimens reveals in a

limited number of regions features such as that shown in figure 6, which are clearly different from those observed in the standardised experiments. The steps visible in this micrograph are consistent with a transgranular propagation of the stress corrosion crack by hydrogen embrittlement (compare with e.g. [11]). The resistance to SCC in continuous immersion after pre-exposure, at a load above the estimated threshold stress in the alternate immersion experiments (see figure 2), reflects the increased susceptibility to stress corrosion in alternate immersion testing.

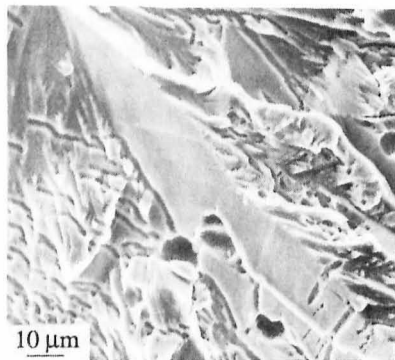


Figure 6. Stepped transgranular fracture in a T651 specimen continuously immersed at an impressed cathodic potential after pre-exposure by alternate immersion.

TABLE I - Results of continuous immersion experiments

Temper	Pre-exposure	Continuous immersion	SCC results
T651	None	at -1100 mV/SCE (100MPa)	3 OK
	1 day I/E at 75 MPa	at free potential	3 OK
	1 day I/E at 75 MPa	at -1100 mV/SCE	11 days, 2 OK
T7451	None	at -1100 mV/SCE (325MPa)	3 OK
	4 days I/E at 325 MPa	at free potential	3 OK
	4 days I/E at 325 MPa	at -1100 mV/SCE	16 days, 2 OK

I/E = alternate immersion (ASTM G44); OK = no failure at 30 days; free potential \approx -900 mV/SCE

3.3 Cross-sectional TEM of SC crack tips

The tips of stress corrosion cracks that propagated in T651 and T7451 ST specimens after 10 days alternate immersion testing at 75 MPa and 310 MPa respectively were examined in cross-section in the TEM. Corresponding observations are presented in figures 7 and 8.

The tips of the stress corrosion cracks observed in the T651 specimen are very fine and localised at or within a few nanometres of grain boundaries (see the characteristic bright field images in figures 7a and 7b, the grain boundary is arrowed in figure 7a). Corrosion was found not to have taken place uniformly along the grain boundaries (see figure 7b) but this could simply reflect the

three-dimensional nature of the crack propagation. The amorphous corrosion product (see inset to figure 7a) visible immediately behind the crack tip corresponds to the consumption of only 100-200 nm of material around the original grain boundary. XEDS analysis indicates that the corroded grain boundary region contains oxygen and chlorine and is enriched in copper with respect to the matrix but is depleted in zinc. The compositional changes for the copper and zinc seem greater than those typically seen at grain boundaries in the peak aged condition where magnesium depletion, rather than the enrichment found in the corroded zone here, is also observed (e.g. [4]). The apparently overaged state of the matrix (note the size of the inter- and intra-granular precipitates) at distances up to about 500 nm from the corroded surface was not typical of the microstructure that was observed in separate TEM foils obtained from positions some millimetres away from the propagating cracks described here.

An overall bright field view of the corroded region which was characterised in the T7451 specimen is presented in figure 8a; higher magnification images for different areas of the grain boundary within it are shown in figures 8b and 8c. In this case the stress corrosion crack is considerably less localised around the grain boundary, seeming if anything to be situated preferentially about 1 μm from it. This observation is confirmed in the bright field micrograph shown in figure 8b, enlarged from the region marked A in figure 8a; one part of the corrosion front abuts the grain boundary but is not propagating preferentially along it. The grain boundary and matrix microstructures at B (see figure 8c), about 2 μm away from the corrosion front, show no morphological features that are substantially different from typical overaged 7150 microstructure. Analysis showed that the Zn:Cu ratio in the surface regions of the alloy examined here is lower than that generally found in the uncorroded state. Moreover, the apparently uncorroded grain boundaries, as shown in figure 8c, are enriched in zinc, which would not normally be expected (e.g. [4]-[6]). The amorphous corrosion product in the fully corroded regions is more straightforward, containing aluminium and oxygen but also minor concentrations of chlorine.

4. Discussion

In the T651 specimens, stress corrosion crack propagation takes place at or within a few nanometres of grain boundaries (see figure 7). The crack progresses in the L-LT plane, regardless of the macroscopic stress orientation, and involves the consumption of about 100 nm of the alloy on either side of the grain boundary in the vicinity of the crack tip (see figure 7). Sub-grain boundaries, even when more favourably oriented with respect to the macroscopic stress state than higher angle boundaries in the L-LT plane, are not preferential sites for crack propagation (see figure 3). We observed no evidence of slip bands or other microstructural features indicative of gross hydrogen embrittlement ahead of the crack tip. These observations are consistent with a process that is controlled by the microstructure in the vicinity of the grain boundary, and thus with studies that demonstrate a correlation between grain boundary microstructure and susceptibility to SCC in copper rich 7xxx alloys. On the basis of the microstructural characterisations of crack paths and crack tips in the T651 specimens, stress accelerated anodic dissolution seems the more plausible propagation mechanism. The observed failure under an impressed cathodic potential, and localised regions of the fracture surface characteristic of transgranular propagation (see table I), would however indicate a dominant susceptibility to hydrogen embrittlement for the T651 temper under continuous immersion. Nevertheless, this failure occurred only after a pre-exposure to an alternate immersion stress corrosion cracking test, and thus in all probability in the presence of a pre-existing stress corrosion crack. For the T651 temper, we thus propose a mixed mechanism of stress corrosion

cracking with both stress assisted anodic dissolution in the vicinity of the grain boundary and hydrogen embrittlement, in this case requiring a pre-crack, as possible propagation mechanisms. The operative mechanism could be modulated as a function of the stress state, potential, and microstructure at the tip of the crack. Furthermore we are concerned about the way in which the matrix microstructure exhibited substantial changes at large distances from the corrosion front in ways which it is difficult to rationalise unless hydrogen in-diffusion allows accelerated ageing. In the T7451 specimens, the cracks also progress in the L-LT plane regardless of loading direction, but the crack tips are less localised at grain boundaries (see figures 4 and 8). Considerably wider crack tips ($\approx 1-2 \mu\text{m}$) were observed in the T7451 foil than in the T651 specimens, though it should be noted that the time elapsed since the last propagation phase of the crack is not clear for this specimen. However, it is clear that the grain boundaries do not represent locally favourable sites for corrosive attack in this specimen. While the matrix and grain boundary microstructure in the vicinity of the cracks did not appear to be structurally different from in the bulk material, the boundary compositions measured in this zone were apparently depleted in copper relative to zinc by comparison with the local matrix Cu:Zn ratio. The microstructural characterisations of crack paths and crack tips in the T7451 temper indicate that the driving force for stress-assisted anodic dissolution at the grain boundaries is considerably reduced with respect to the T651 temper, though propagation in the L-LT plane is still favoured. The observed failure under an impressed cathodic potential, but only after 4 days pre-exposure to an alternate immersion stress corrosion cracking test (see table I), demonstrates a slight susceptibility of the T7451 temper to hydrogen embrittlement in continuous immersion. We thus postulate that this overaged temper is desensitised with respect to stress-assisted anodic dissolution at the grain boundaries, but still slightly sensitive to hydrogen embrittlement in the vicinity of grain boundaries given the presence of a pre-crack.

5. Conclusions

Detailed microstructural analysis of crack tips, and in particular cross-sectional TEM, provides valuable information on crack propagation in peak aged and overaged tempers of 7150 alloy. The crack tip is localised at or within a couple of nanometres of the grain boundary in the T651 temper, and at about $1-2 \mu\text{m}$ of grain boundaries in the T7451 crack tips examined. Crack propagation takes place in the L-LT plane, irrespective of loading direction between 0 and 45° to the ST direction, demonstrating the importance of detailed grain boundary microstructure to the SCC process. No particular evidence for hydrogen embrittlement was obtained from these microstructural characterisations, though the sensitivity of the alloy in conditions favouring hydrogen embrittlement was demonstrated.

Acknowledgements :

Thanks are due to Ms Sille Grjotheim for the performance of stress corrosion cracking tests, to V. Chastagnier and C. Rard for SEM work, to Max Reboul for useful discussions, and to Pechiney CRV for permission to publish.

References:

1. N.J.H. Nolroyd (1989) Proc. of Environment-Induced cracking of metals, NACE, pp 311-345.
2. T.D. Burleigh (1991) Corrosion **47**, pp 89-98.

3. M.C. Reboul, T. Magnin, and T.J. Warner (1992) Proc. of the 3rd International conference on aluminum alloys, Trondheim, Norway (22-26 June 1992), pp 453-460.
4. B.V.N. Rao (1981) *Met. Trans.* **12A**, pp1356-1359.
5. P. Doig, P.E.J. Flewitt, and J.W. Eddington (1977) *Corrosion* **33**, pp 217-221.
6. M.B. Hall and J.W. Martin (1994) *Z. Metallkunde* **85**, pp134-139.
7. J.P. Park (1988) *Mat. Sci. Eng.* **A103**, pp 223-226.
8. P.K. Poulouse, J.E. Morall, A.J. McEvily (1972) *Met. Trans.* **3**, p. 1393.
9. M.O. Speidel, *Fundamental aspects of stress corrosion cracking*, p561.
10. M. Talianker and B. Cina (1989) *Met. Trans.* **20A**, pp2987-2092.
11. A.W. Thompson, M.P. Mueller, and I.M. Bernstein (1993) *Met. Trans.* **24A**, pp 2569-2575.
12. J. Albrecht, A.W. Thompson, I.M. Bernstein, (1979), *Metall. Trans.* **10A**, p 1759.
13. D. Najjar, R. Chieragatti, T. Magnin, and T.J. Warner (1993), Proc. of NACE fall conference.
14. S.B. Newcomb, C.B. Boothroyd, and W.M. Stobbs (1985) *J. Microsc.* **140**, 195-217.

Figure 7 - Bright field TEM micrographs showing the typical microstructure of a peak aged ST specimen around corroded grain boundary crack tips formed after 10 days alternate immersion at 75 MPa. The inset diffraction pattern in a) was taken from the amorphous corrosion product formed nearer the surface of the alloy.

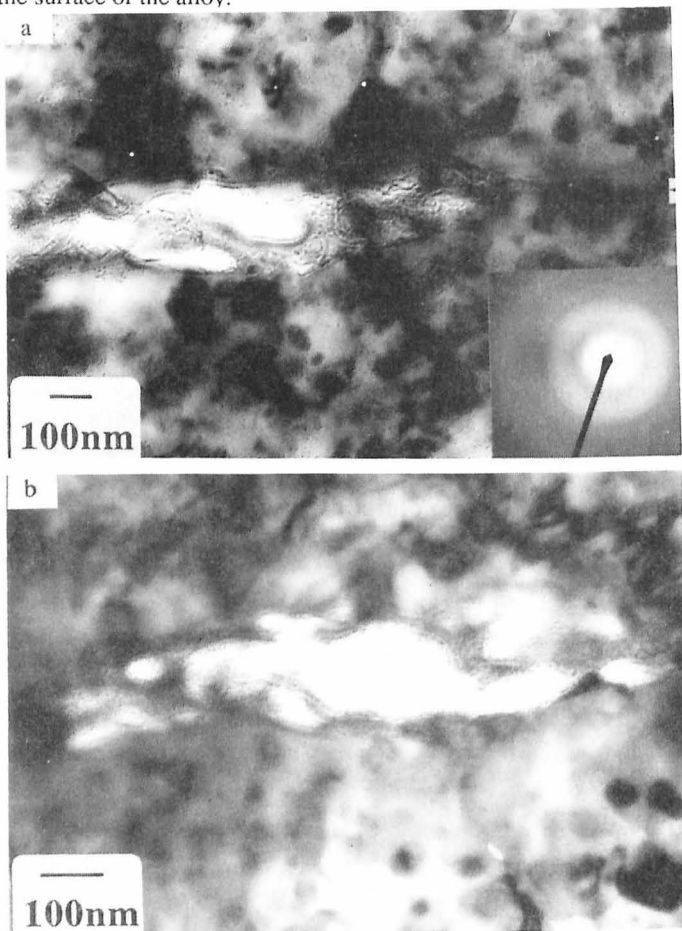


Figure 8 - Bright field TEM micrographs of a corrosion front formed after 10 days alternate immersion at 310 MPa in an overaged specimen showing a) a low magnification view of the whole region and higher magnification micrographs enlarged from b) region A and c) region B in figure 8a.

